Review article

Yuttana Intaravanne and Xianzhong Chen*

# Recent advances in optical metasurfaces for polarization detection and engineered polarization profiles

https://doi.org/10.1515/nanoph-2019-0479
Received November 25, 2019; revised January 5, 2020; accepted January 26, 2020

**Abstract:** Like amplitude, phase and frequency, polarization is one of the fundamental properties of light, which can be used to record, process and store information. Optical metasurfaces are ultrathin inhomogeneous media with planar nanostructures that can manipulate the optical properties of light at the subwavelength scale, which have become a current subject of intense research due to the desirable control of light propagation. The unprecedented capability of optical metasurfaces in the manipulation of the light's polarization at subwavelength resolution has provided an unusual approach for polarization detection and arbitrary manipulation of polarization profiles. A compact metasurface platform has been demonstrated to detect polarization information of a light beam and to arbitrarily engineer a polarization profile that is very difficult or impossible to realize with conventional optical elements. This review will focus on the recent progress on ultrathin metasurface devices for polarization detection and realization of customized polarization profiles. Optical metasurfaces have provided new opportunities for polarization detection and manipulation, which can facilitate real-world deployment of polarization-related devices and systems in various research fields, including sensing, imaging, encryption, optical communications, quantum science, and fundamental physics.

**Keywords:** optical metasurfaces; geometric phase; polarization detection; polarmetric imaging; vector beams polarization profile manipulation.

***Corresponding author: Xianzhong Chen,** School of Engineering and Physical Sciences, Heriot-Watt University, Edinburgh, UK, e-mail: x.chen@hw.ac.uk. https://orcid.org/0000-0001-7521-1548
**Yuttana Intaravanne:** School of Engineering and Physical Sciences, Heriot-Watt University, Edinburgh, UK

## 1 Introduction

Like amplitude, phase and frequency, polarization is one of fundamental properties of light. The polarization of light refers to a direction in which an electric component of this field oscillates. The polarization of sunlight is usually random, meaning that the orientation of the electric field is independent from one beam to another. However, the light can become polarized in a specific direction using a polarizer. Polarization can also be changed upon reflection off a surface. Polarization has found many applications in our daily life, including polarized sunglasses, polarization cameras, and three-dimensional (3D) cinema. Polarization contains valuable information about the imaged environment (e.g. material and tissue properties, surface roughness, shape and texture of reflecting surfaces, the orientation of light emitters, or the optical activity of various materials) [1–5], which is typically unavailable in color, intensity and spectral content. Polarization detection is a very important research field. The polarization state of light over a scene of interest can be measured by polarimetric imaging, which has led to many applications ranging from astronomy and remote sensing to biology (e.g. early cancer formation), medicine [2–5] and microscopy [5]. However, their applications are still limited since many polarization elements are involved, which result in a large volume and high cost. To meet the growing requirement of device miniaturization and system integration, miniaturized optical devices and compact detection systems are desirable.

By contrast, how to generate a light beam with a predesigned polarization profile is also very important. A vector beam has an inhomogeneous distribution of polarization in the transverse plane perpendicular to the propagation direction. Vector beams have been recognized as a promising future technology in quantum memories, particle trapping, and high-resolution lithography [6–9]. However, despite tremendous advances in the fundamental principles of vector beams (e.g. Mobius strip [10], Poincaré sphere beams [11]), the real-life applications remain

limited, mainly because of the complexity of the experimental system and the inability to arbitrarily manipulate the polarization state of light at the subwavelength scale. Many devices such as liquid-crystal q-plates [12, 13] have been proposed to generate vector beams such as widely explored radially and azimuthally polarized beams. However, these devices could not be straightforwardly downsized, preventing widespread applications in integrated optics. Furthermore, the limitations of poor resolution and low damage threshold still need to be overcome for practical applications. There are numerous challenges, either fundamental or technological, in building devices that are compact, efficient, and integrable.

Optical metasurfaces are ultrathin inhomogeneous media with planar structures of nanopatterns that can manipulate the optical properties of light at the subwavelength scale, which have become a current subject of intense research due to the unprecedented control of light propagation. Metasurfaces have enabled high-efficiency phase and polarization control with large gradients, enabling a plethora of ultrathin optical devices, including metalenses [14–33], holograms [34–43], orbital angular momentum state generators [44–52], color filters [53–62] and so on. Recently, the study of light-matter interactions on nonlinear optical metasurfaces has attracted extensive interest [63–70]. Optical metasurfaces have been extended to nonlinear optical processes, such as second [71–76], third [77–80], and high [81] harmonic generation, and broadband optical frequency mixers [82]. The nonlinear processes in the meta-atoms [83, 84] have led to many nonlinear applications such as nonlinear holography [85, 86], nonlinear spin-orbital interactions of light [87], nonlinear metalenses [88], and nonlinear image encryption [89]. In addition, metasurfaces have provided a new opportunity to add a new degree of freedom (polarization information) in current imaging systems due to their potential for vertical integration and design flexibility [90–93]. Various compact metasurface devices for polarization detection have been developed [47, 94–109]. Furthermore, to overcome the present technical limitation of resolution and fundamental challenge of arbitrary polarization manipulation, metasurfaces have also been used to precisely generate the spatially variant polarization states of a laser beam with an ultrathin metasurface [110–116]. This review concentrates on the applications of metasurfaces in the polarization detection and arbitrary polarization manipulation. The impact of these ultrathin devices may be substantial in a variety of fields, including encryption, imaging, optical communications, photonics, quantum science, and fundamental physics. The review is organized as follows. In Section 2, we first overview the background of polarization detection and the advantages of optical metasurfaces, then move on to circular polarization detection, full polarization detection and their applications in polarimetric imaging, which have recently stimulated worldwide research interest in optical metasurfaces. In Section 3, we review arbitrary polarization manipulation and its applications in image concealment based on the Malus' Law, including high-resolution grayscale images, quick response (QR) codes, color images, polarization-sensitive holograms and images in second harmonic generation (SHG) waves. In Section 4, we give concluding remarks and a personal outlook on future research directions.

# 2 Polarization detection

## 2.1 Background

Polarization detection has been used for a wide variety of applications. Based on the measurement and interpretation of the polarization of light waves, polarimetry has been applied in many areas of science and technology [117], ranging from ellipsometry [118, 119], remote sensing [120] to polarization light scattering [121] and ophthalmic polarimetry [122]. For example, in defense and security, polarization information can be used to pick out artificial materials against natural surfaces. In atmospheric monitoring, it can be used to track the size and distribution of particles in the atmosphere, which can be used to monitor air quality. To measure the polarization state of a light beam, many polarization elements (e.g. polarizers, waveplates, polarization modulators) are usually employed and placed in a beam of light in front of a power meter. The traditional measurement systems have advantages in measuring speed and accuracy, but their applications are still limited due to the various polarization elements and complicated data processing system adopted, leading to a large volume and high cost. The metasurface approach differs from previous approaches in that the phase change occurs abruptly at the interface rather than slowly evolving in, for example, a birefringent material commonly used in bulky polarization optics. Consequently, this can lead to further miniaturization and a greater potential for system integration. The ultrathin circular polarizers [123–125] and polarization rotators [126, 127] based on metamaterials have been developed recently. As planar metamaterials, metasurfaces [128–130] do not require complicated 3D nanofabrication techniques, but can convert the linearly polarized incident light to its cross polarization [116], or

convert a circularly polarized light to its opposite handedness [14, 15, 131–133]. Metasurfaces have been used in circular polarization detection [94–99], full polarization measurement [47, 100–109] and polarimetric imaging [90–93].

## 2.2 Circular polarization detection

Figure 1A shows the schematic of circular polarization detection based on a phase gradient metasurface consisting of spatially variant metallic nanorods [94]. All gold nanorods on indium tin oxide-coated glass substrate have identical geometric parameters with spatially variant orientations. The angular orientation of each nanorod varies along the x-direction with an increment of π/8 in a clockwise rotation, but remains invariant in the y-direction. Hence, each period in the x-direction contains eight nanorods, the orientations of which change from 0 to π, which generate the additional Pancharatnam-Berry phase shifts ranging from 0 to 2π. When an incident light beam passes through the metasurface, the refracted light emerging from the metasurface is the sum of three terms with separate amplitudes: the regularly refracted light with the same polarization of the incident light, the anomalously refracted left circular polarization (LCP) light and the right circular polarization (RCP) light. The ellipticity and the handedness of the incident light can be deduced from the relative intensities of the last two terms. Interestingly, since the refracted LCP and RCP light diverge naturally from each other, the metasurface can also be used as a circular polarization beam splitter, the split angle of which is determined by controlling the spatial distribution of the nanorods in the metasurface.

The low conversion efficiency can be dramatically improved by using a dielectric metasurface [95]. To develop such a planar chirality-distinguishing beam splitter with a large extinction ratio, a dielectric metasurface consisting of amorphous silicon nanofins on a glass substrate was used. Each nanofin thus acts like a wave-plate with phase retardation of φ and its transmission can be modeled by Jones matrix. Birefringence of the

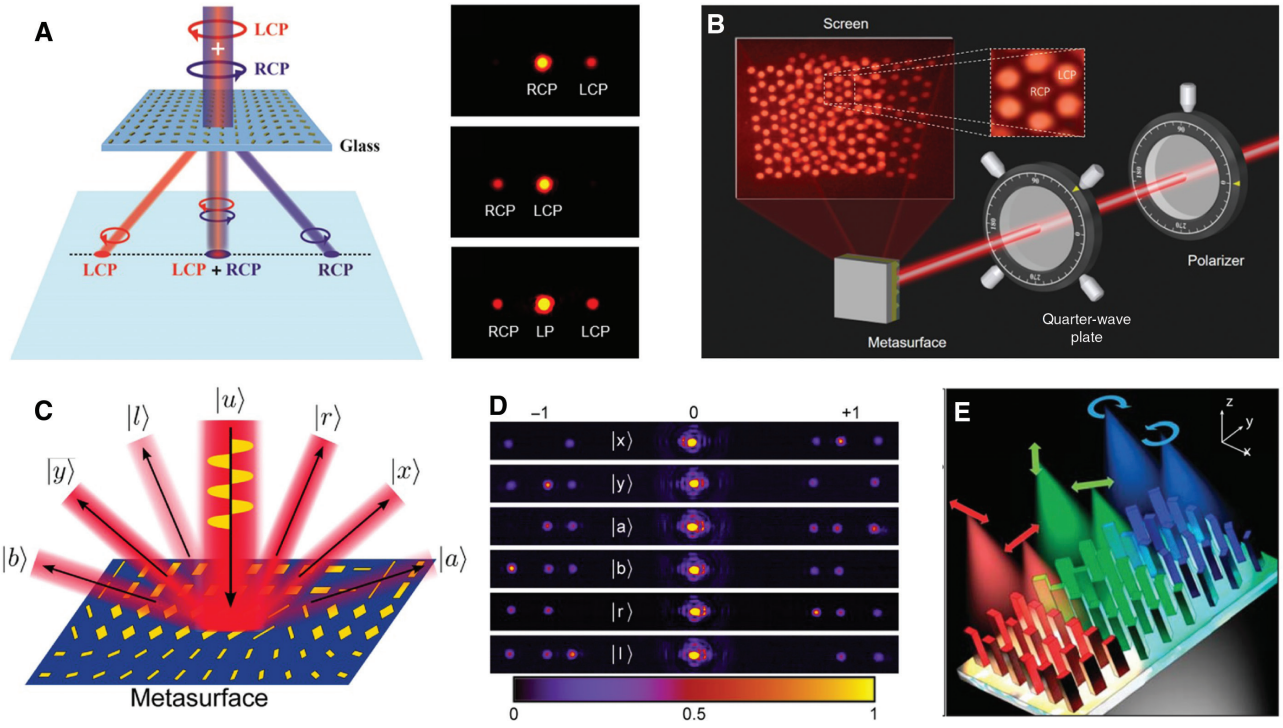


**Figure 1:** Optical metasurfaces for polarization measurement.
(A) Left: schematic to show the polarization of the refracted light after a completely polarized light beam passing through the metasurface. Right: experimental results of the refracted light spots on the transmission side of the metasurface for incident light with different polarization states [94]. (B) Schematic of the experimental setup to demonstrate the polarization measurement based on the reconstructed holographic images [98]. (C) Illustration of the full polarization measurement based on a reflective metasurface consisting of triple layers: nanorods on the top, metal film at the bottom and the dielectric layer sandwiched between them. (D) Experimental results in (C) for an incoming beam with an unknown polarization state can allow one to determine the Stokes parameters [100]. (E) Three-dimensional illustration of a superpixel that can focus different polarizations to different spots [107]. Reprint permission obtained from [94, 98, 100, 107].

wave-plate originates from the asymmetric cross-section (length > width) of the nanofin. In this design, there are only three possible diffracted orders ($m = 0, \pm 1$). The power in the $m = 0$ diffracted order does not depend on the phase difference between incident electric field components. By contrast, the powers of the $m = \pm 1$ orders are sensitive to the phase difference. This characteristic enables us to identify the handedness of the incident light through observation of the $m = \pm 1$ orders. Furthermore, the fraction of power that is in the $m = \pm 1$ orders vs. the $m = 0$ order can be varied from zero to 100% by the appropriate choice of phase retardation $\varphi$. The latter can be achieved by adjusting the nanofin dimensions or changing the surrounding refractive index. If $\varphi$ is an odd multiple of $\pi$, the output is entirely first order ($m = \pm 1$), while if $\varphi$ is an even multiple of $\pi$, the output is entirely zero-th order ($m = 0$).

Recently, a polarization-sensitive hologram approach was also used to measure the polarization state of a light beam [98]. This approach is based on the reconstructed holographic images upon the illumination of the light beam. When the light beam with pure LCP is incident on the metasurface, a clear holographic image (graphene pattern) is seen. A holographic image of the same graphene pattern with a rotated angle is observed when the polarization state of the light is changed from LCP to RCP. The two holographic images overlap upon the illumination of the light beam with linear polarization, since it can be decomposed into LCP and RCP beams with equal components. For a light beam with elliptical polarizations, the intensities of the two holographic images for LCP and RCP are different, because the two components for LCP and RCP beams are different. Due to the unique pattern of the graphene structures, the polarization state of the incident light can be determined by measuring the intensities of the two neighboring light spots in the overlap area of holographic images. The dynamic polarization change of a light beam can be quickly estimated based on the rise and fall of intensities of the reconstructed holographic images, providing a fast and elegant polarization measurement method based on polarization-sensitive metasurface holograms.

## 2.3 Full polarization measurement

To completely characterize the polarization state of light, three metasurfaces constituting the metagratings were used. They can work independently due to different supercell periodicities (different diffraction angles) [100]. This point was validated by considering the diffraction spots of the metagrating. For the six polarizations, one diffraction order is in turn suppressed whereas the remaining two pairs of diffraction spots show (approximately) equal splitting. In addition, considering a multitude of polarization states along the main axes of the Poincaré sphere, the associated diffraction contrasts (each obtained by averaging three successive measurements) can replicate reasonably well the unit sphere, with points covering all octants of the 3D parameter space. A metagrating allows the determination of the polarization state of the incident light in one measurement without the need of additional polarizers. This is very attractive approach since the metagrating constitutes a fast, simple, and compact way to determine a probe signal's unknown polarization state.

However, reflective metasurfaces are not compatible with most transmission type optical elements. To solve this issue, a metasurface consisting of dielectric birefringent nanopost structures are used [107]. The device was designed to split and focus light to six different pixels on an image sensor for three different polarization bases. This allows for complete characterization of polarization by measuring the four Stokes parameters over the area of each superpixel, which corresponds to the area of six pixels on an image sensor. There are several representations for polarization of light. Among them, the Stokes vector formalism has some conceptual and experimental advantages, since it can be used to represent light with various degrees of polarization and can be directly determined by measuring the power in certain polarization bases. This group experimentally demonstrated the ability of the metasurface masks to correctly measure the polarization state for different input polarizations. In addition, the division of a focal plane metasurface mask was used to form an image of a complicated polarization object, showing the ability to make a polarization camera. An optical metasurface with the ability to fully control the phase and polarization of light can perform the full polarization measurement over a much smaller volume.

## 2.4 Polarimetric imaging

Polarimetric imaging is the measurement of the polarization state of light over a scene of interest [90]. While spectral and hyperspectral imaging techniques provide information about the molecular and material composition of a scene, polarimetric imaging contains valuable information about the shape and texture of reflecting surfaces, the orientation of light emitters, or the optical activity of various materials.

Figure 2A shows the schematic for chiral imaging. Chiral materials, which are common in biological compounds, can be classified from consequential analysis of circular polarizations. The vast majority of biologically active compounds, ranging from amino acids to essential nutrients such as glucose, possess intrinsic handedness. This in turn gives rise to chiral optical properties, providing a basis for detecting and quantifying enantiospecific concentrations of these molecules. Harvard University experimentally demonstrated the chiral imaging capabilities and spatially resolved chiral spectroscopy with a single planar lens. Conventionally, this cannot be achieved using single optical components unless multiples of them are stacked together into a bulky system. The building blocks of a multispectral chiral lens are comprised of two nanofins shown in blue and green. The required phase for focusing light is imparted based on the Pancharatnam-Berry phase via rotation of nanofins. The focusing efficiency is maximized when each nanofin acts as a half-wave plate, which converts circularly polarized input light into transmitted light with opposite helicity.

Figure 2B shows a metasurface chip that can assist in detecting the intensity of one specific polarization state, therefore, one can attain a set of Stokes parameters simultaneously with the absence of optical components in front of the detector (a COMS camera) [91]. Samples with chiral properties were measured using both on-chip polarimetry and commercial ellipsometry.

Very recently, matrix Fourier optics was proposed for treating polarization in paraxial diffractive optics [92]. This formalism is a powerful generalization of a large body of past work on optical elements in which polarization

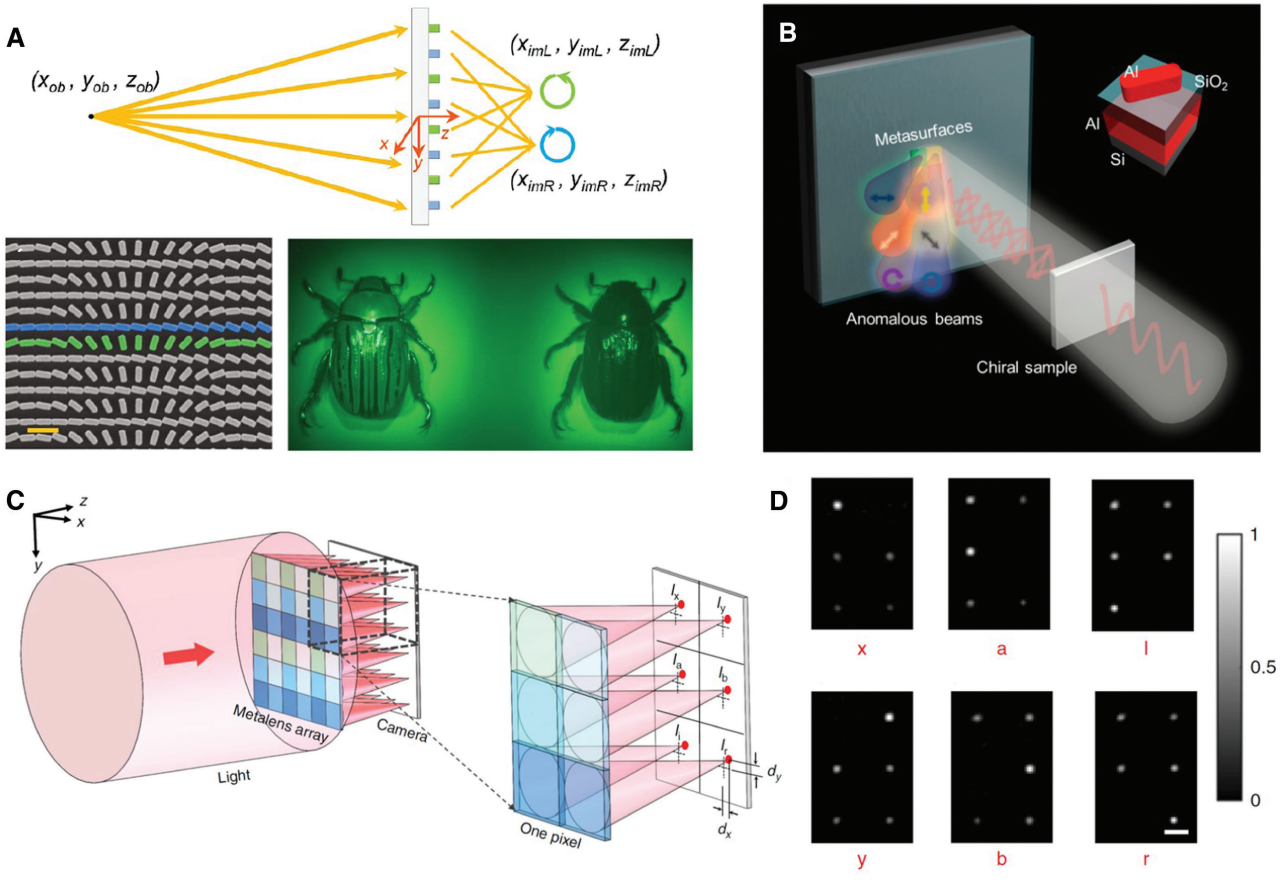


**Figure 2:** Optical metasurfaces for polarimetric imaging and wavefront sensors.
(A) Top: schematic diagram illustrating the imaging principle of the multispectral chiral lens (MCHL) where left circular polarization (LCP) and right circular polarization (RCP) light from the same object at coordinates ($x_{ob} = 0$, $y_{ob} = 0$, $z_{ob} = -18$ cm) are focused into two spots, ($x_{imL}$, $y_{imL}$, $z_{imL}$) and ($x_{imR}$, $y_{imR}$, $z_{imR}$), respectively. Bottom left: scanning electron microscopy image of the fabricated MCHL. Scale bar: 600 nm. The two interlaced arrays of nanofins are false-colored. Bottom right: experimental results from [90]. (B) Schematic illustration of the on-chip polarimetry with integrated metasurfaces that can work at visible light [91]. (C) Scheme of the generalized Hartmann–Shack beam profiler. Each pixel of the array shown on the left consists of six different polarization-sensitive metalenses and (D) measured images of the resulting focal spots for incident horizontal or vertical linear polarization ("x" and "y"), diagonal linear polarization ("a" and "b"), and circular polarization ("l" and "r") [93]. Reprint permission obtained from [90, 91, 93].

may vary spatially. Moreover, it suggests a path to realizing many polarization devices in parallel using a single optical element. It can be used to design diffraction gratings, the orders of which behave as polarizers for an arbitrarily selected set of polarization states, a new class of optical element. Polarized light from a photographic scene is incident on the grating inside of a camera. The polarization is "sorted" by the specially designed subwavelength metasurface grating. When combined with imaging optics (a lens) and a sensor, four copies of the image corresponding to four diffraction orders are formed on the imaging sensor. These copies have each, effectively, passed through a different polarizer, the functions of which are embedded in the metasurface. The four images can be analyzed pixel-wise to reconstruct the four element Stokes vector across the scene. Several examples were demonstrated at 532 nm, both indoors and outdoors.

Figure 2C and D show a dielectric metalens system which can be used not only to measure phase and phase-gradient profiles of optical beams (as a conventional Hartmann-Shack array), but also to measure the spatial polarization profiles at the same time [93].

# 3 Arbitrary polarization manipulation

## 3.1 Background

We can not only measure the polarization state of light, but also can generate a light beam with an engineered polarization profile. A light beam usually has a homogeneous polarization profile after passing through a polarizer, but a vector beam has an inhomogeneous distribution of polarization in the transverse plane perpendicular to the propagation direction. Metasufaces have been demonstrated to generate vector beams, such as radially or azimuthally polarized cylindrical beams, and arbitrary spatial polarization profiles. Recently, metasurfaces have been demonstrated to encode images in the polarization profiles [110–116]. In order to overcome the present technical limitation of resolution and fundamental challenge of arbitrary polarization manipulation, high capacity information can be encoded by a light beam by precisely manipulating the spatially variant polarization states of a laser beam with an ultrathin metasurface. A metasurface platform for the arbitrary polarization manipulation has been used to encode various types of images, including a high-resolution grayscale image [111], a QR code [112] and a color image [113], which has been recently extended to nonlinear metasurfaces [116].

## 3.2 Image hidden in the polarization profile of a light beam

The structured beam that can be used to hide an image was created by a metasurface illuminated by the laser light at normal incidence [111]. According to the Malus' Law, when a linearly polarized light beam (generated by a polarizer) with an intensity $I_0$ passes through an analyzer (linear polarizer), the transmitted light intensity is proportional to the square of the cosine of angle $\theta$ between the transmission axes of the analyzer and the polarizer, i.e. $I = I_0 \cos^2\theta$. Thus, the required linear polarization profile for a hidden image is determined by its intensity profile. The predesigned linear polarization topology can be generated by a coherent superposition of two planar circularly polarized beams with opposite handedness, which can be realized by a reflective metasurface.

To hide a portrait of James Clark Maxwell, a single reflective metasurface was used to continuously manipulate the superposition of two beams with opposite circular polarization states. The reflective metasurface consists of a gold ground layer, a silicon dioxide spacer layer, and a top layer of gold nanorods. The generated structured light has a very specific polarization in the light beam, thus the light field oscillates differently for different parts of the beam. In order to visualize the hidden image in the polarization topology of the laser beam, the grayscale of the image was revealed by using an analyzer (linear polarizer). In doing so, the spatially-variant polarization profile of the laser beam cannot be observed directly, but its existence can be indirectly confirmed through the intensity profile (grayscale image) behind the analyzer. Figure 3A shows the simulation and experiment results. Because the theoretical amplitudes of the two beams are exactly the same, no image is observed in the beam without the aid of the analyzer. The experimental result indicates that the image-hidden functionality is unambiguously realized. QR codes are 2D barcodes usually consisting of black white patterns with a spatially varying intensity profile, which can be processed by a QR reading machine such as a smart phone. QR codes have been widely used in many fields, including product identification, item tracking, and document management. To keep pace with the continued miniaturization of devices and the daunting increase in the volume of information, new approaches to generate QR codes are desirable. Figure 3B shows the experimental

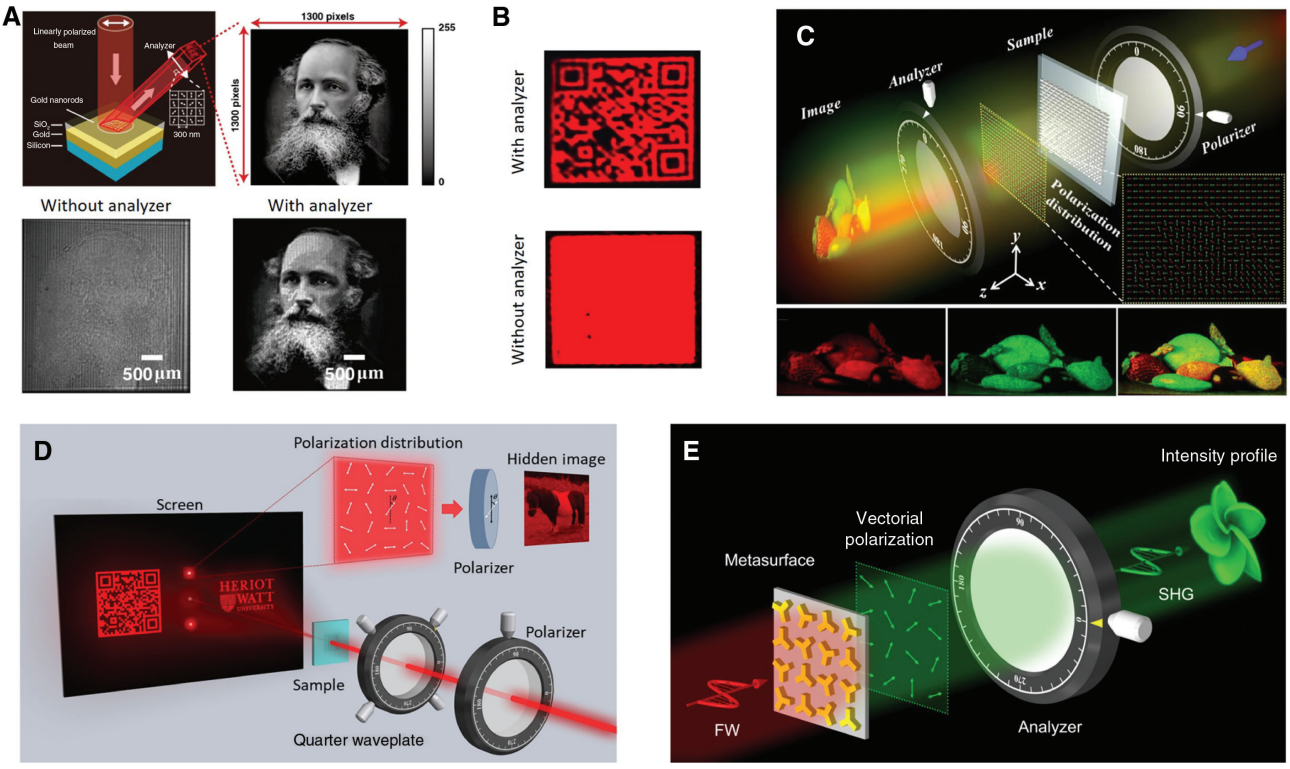


**Figure 3:** Optical metasurfaces for engineered polarization profiles.
(A) Schematic for hiding a high-resolution grayscale image. Under the illumination of linearly polarized light, a grayscale image is hidden in the polarization profile of a reflected beam from the metasurface and revealed by a linear polarizer (analyser) [111]. (B) Generation of quick response (QR) code for anticounterfeiting [112]. (C) Top: schematic for the polarization encoded color image. Bottom: experimental results for incident light with red, green and two colors [113]. (D) Schematic of the multichannel metadevice for anticounterfeiting and encryption [115]. (E) Schematic of nonlinear vectorial metasurface for optical encryption [116]. Reprint permission obtained from [111–113, 115, 116].

result of a QR code, which is hidden in the polarization profile of a light beam [112].

## 3.3 Color image embedded in a metasurface

A metasurface platform has been demonstrated to simultaneously encode color and intensity information into the wavelength-dependent polarization profile of a light beam [113]. Unlike typical metasurface devices in which images are encoded by phase or amplitude modulation, the color image here is multiplexed into several sets of polarization profiles, each corresponding to a distinct color, which further allows polarization-modulation-induced additive color mixing. This unique approach features the combination of wavelength selectivity and arbitrary polarization control down to a single subwavelength pixel level. Upon the illumination of a linearly polarized light beam with multiple wavelengths, a color image is revealed after the light beam passes through a dielectric metasurface and a linear optical polarizer. The dielectric metasurface consists of silicon nanoblocks "meta-atoms" with different in-plane orientations and sizes on a fused silica substrate, which can be used to generate the desired polarization profile for two different colors, with a locally controlled intensity profile. Two wavelength-selective polarization profiles were designed to produce the polarization-encoded color images based on additive color mixing. Each supercell responds to a specific wavelength upon the illumination of a light beam containing red and green colors. The supercell represents a pixel of a mixed-color image with the brightness of each color being individually controlled. Figure 3C shows the schematic and the experimental results upon the illumination of linearly polarized red, green and dual-color light. This approach provides a novel route to hide a high-resolution grayscale image in the polarization topology of a laser beam. The dielectric metasurface having the ability to encode a spatially-varying and wavelength-selective polarization profile may provide a viable route for generating structured beams that unveil high-resolution color images with well-defined brightness and contrast.

### 3.4 Polarization-sensitive hologram with a hidden image

Driven by high profits, the potential harm and risks from the production and sale of fraudulent goods are big issues in our world. Much effort has been devoted to anticounterfeiting technologies. However, conventional methods for anticounterfeiting, such as commonly used holograms, are not very effective since they are outdated and easy to duplicate. Researchers have been looking for alternative holograms with unique properties that are not easy to design and are difficult to copy. Figure 3D shows a multichannel device that can realize an image-switchable hologram and nonuniform polarization profile for anticounterfeiting in different channels [115]. By integrating different functionalities (helicity multiplexed holograms and arbitrary polarization manipulation) onto the same metasurface device, a highly versatile ultracompact multichannel device with minimal spatial footprint can be achieved. Two separate holographic images are observed when the device is illuminated by a circularly polarized light beam (RCP or LCP). The holographic images will overlap when a light beam with elliptical polarization impinges on the device, since any polarized light beam can be decomposed into two beams with opposite circular polarization states. The rise and fall of intensities of two overlapping images is determined by the ellipticity of polarized light. The intensities of two overlapping images are the same for the linearly polarized light, since it contains an LCP light beam and a RCP light beam with the same components. When the incident light is linearly polarized and the analyzer is applied, the overlapped images will still exist, but the brightness is decreased. The intensity of the "QR code" dominates for the right-hand elliptically polarized light. Finally, two separate images are obtained again, but they are swapped and flipped. The second functionality of the developed device is an arbitrary polarization profile for the hidden image. Upon the illumination of linear polarization light along the horizontal direction, no image is obtained without the analyzer due to the uniform intensity distribution. The hidden image is decoded correctly only when the transmission axis of the analyzer is along the vertical direction. Hence, the transmission axis of the analyzer plays an important role in the decryption process.

### 3.5 Nonlinear vectorial metasurface

Nonlinear optical processes, such as second, third, and high harmonic generation, and broadband optical frequency mixers are extensively investigated by using both plasmonic and dielectric metasurfaces. A nonlinear optical metasurface was demonstrated to locally manipulate the polarization states of the SHG wave and encode a high-resolution image in the polarization profile accordingly [116]. To encrypt image information into nonlinear optical devices, the nonlinear plasmonic meta-atoms with threefold rotational (C3) symmetry were utilized to construct the nonlinear metasurface. For a meta-atom with m-fold rotational symmetry, upon illumination along its rotational axis by circularly polarized fundamental waves (FWs), the allowed orders of nonlinear harmonic generation are restricted by the selection rule to $n = lm \pm 1$, where l is an integer and the "+" and "−" signs indicate that the harmonic waves and the FWs possess the same and opposite spin states, respectively. Detailed explanation is available in the references [80, 83, 84]. Therefore, the C3 meta-atom can selectively produce SHGs with opposite handedness to that of the incident circularly polarized FW. More significantly, the nonlinear polarizability of the meta-atoms can be continuously manipulated by varying their orientations. As a result, a nonlinear geometric phase, $-3\sigma\theta$, is simultaneously imparted to the SHG wave, where $\sigma = \pm 1$ is the handedness of the incident FW and $\theta$ is the angle by which the C3 meta-atom is rotated with respect to the laboratory frame. By using this characteristic, image information can be encrypted into a polarization profile of the SHG waves. With such an encoding process, one can effectively control the polarization states of the SHG wave in the transverse plane. Using a linear polarizer, the polarization profile can be converted into an intensity profile, which allows for easier observation.

## 4 Conclusions and outlook

Polarization detection is vital in our modern society for the processing and transmission of information. To keep pace with the continued miniaturization of devices and the daunting increase in the volume of information, new detection and imaging devices and new approaches to process and transmit information are required. The unprecedented capability of optical metasurfaces in the manipulation of light propagation has provided unusual approaches for the development of ultrathin, ultraflat, compact optical devices for polarization measurement, enabling a polarization imaging system without moving parts, bulk polarization optics, and specially patterned camera pixels. Metasurface-based polarization imaging may find applications in remote sensing, atmospheric science, machine

vision, and even on-board autonomous vehicles. The only other main component needed for complete polarimetric beam profiling is a standard camera. Metasurface structures and polarimetric devices have exhibited various advantages, including ultracompact footprint, easy on-chip integration, manufacturing scalability, and dispersion control. Metasurfaces hold great promise for facilitating chip-integrated polarimeters and polarimetric imaging systems for quantum computing and information processing, biomedical imaging, and sensing applications. Imaging the polarization of light scattered from an object provides an additional degree of freedom for gaining information from a scene. The polarization change can produce specific contrasts to reveal hidden information, which has been used in material science, object detection, surface quality analysis, enhanced vision, target detection, medicine and microscopy, and biomedical diagnosis. For example, it can help us in the 3D reconstruction of an object, to estimate its depth, texture and shape, and to identify the boundary between two different materials, even if they are the same shape and color.

Metasurface-enabled arbitrary polarization manipulation is a new research field. The hidden images in the polarization profiles demonstrate the rich polarization structure that a light beam can possess at subwavelength scales. The precise control over the polarization state of light can be faithfully mapped onto the intensity profile for each color. The encoding approach for polarization and color may open a new avenue for novel, effective color display elements with fine control over both brightness and contrast, and may have significant impact for high-density data storage, information security, and anticounterfeiting. The dielectric metasurface having the ability to encode a spatially-varying and wavelength-selective polarization profile may provide a viable route for generating structured beams that unveil high-resolution color images with well-defined brightness and contrast.

Polarization-related ultrathin nanodevices, nanophotonic systems, and integration of multifunctional capability into ever smaller and more flexibly connected and deployable units will be an immensely important research topic in the years ahead. To reduce the fabrication cost and facilitate industrial uptake, the computer-chip fabrication technology can be used to massively produce such devices. Metasurface technology can enable tasks that are not possible with classical methods, promising advances in a variety of scientific fields impacting our everyday lives. The rapid development of metasurfaces for polarization detection and manipulation and its large impact have shown that metasurfaces can excite scientists, engineers, industry, and the actual economy.

**Acknowledgments:** This project is supported by the Engineering and Physical Sciences Research Council of the United Kingdom (Grant Ref: EP/ P029892/1, Funder Id: http://dx.doi.org/10.13039/501100000266). Y.I. acknowledges the support from the Ministry of Science and Technology (Thailand), and the Royal Thai Embassy in London (UK).

## References

[1] Tyo J, Goldstein DL, Chenault D, Shaw J. Review of passive imaging polarimetry for remote sensing applications. Appl Opt 2006;45:5453–69.
[2] Bailey J, Chrysostomou A, Hough J, Gledhill T. Circular polarization in star-formation regions: Implications for biomolecular homochirality. Science 1998;281:672–4.
[3] Smidlehner T, Piantanida I, Pescitelli G. Polarization spectroscopy methods in the determination of interactions of small molecules with nucleic acids - tutorial. Beilstein J Org Chem 2018;14:84–105.
[4] Ghosh N, Vitkin AI. Tissue polarimetry: concepts, challenges, applications, and outlook. J Biomed Opt 2011;16:1–30.
[5] Wang Y, He H, Chang J, et al. Differentiating characteristic microstructural features of cancerous tissues using Mueller matrix microscope. Micron 2015;79:8–15.
[6] Parigi V, D'Ambrosio V, Arnold C, Marrucci L, Sciarrino F, Laurat J. Storage and retrieval of vector beams of light in a multiple-degree-of-freedom quantum memory. Nat Commun 2015;6:7706.
[7] Ng J, Lin Z, Chan CT. Theory of optical trapping by an optical vortex beam. Phys Rev Lett 2010;104:103601.
[8] D'Ambrosio V, Nagali E, Walborn SP, et al. Complete experimental toolbox for alignment-free quantum communication. Nat Commun 2012;3:961.
[9] Bauer T, Orlov S, Peschel U, Banzer P, Leuchs G. Nanointerferometric amplitude and phase reconstruction of tightly focused vector beams. Nat Photonics 2013;8:23–7.
[10] Bauer T, Banzer P, Karimi E, et al. Observation of optical polarization Möbius strips. Science 2015;347:964–6.
[11] Naidoo D, Roux FS, Dudley A, et al. Controlled generation of higher-order Poincaré sphere beams from a laser. Nat Photonics 2016;10:327–32.
[12] Cardano F, Karimi E, Slussarenko S, Marrucci L, de Lisio C, Santamato E. Polarization pattern of vector vortex beams generated by q-plates with different topological charges. Appl Opt 2012;51:C1–6.
[13] Rumala YS, Milione G, Nguyen TA, et al. Tunable supercontinuum light vector vortex beam generator using a q-plate. Opt Lett 2013;38:5083–6.
[14] Chen X, Huang L, Mühlenbernd H, et al. Dual-polarity plasmonic metalens for visible light. Nat Commun 2012;3:1198.
[15] Chen X, Huang L, Mühlenbernd H, et al. Reversible three-dimensional focusing of visible light with ultrathin plasmonic flat lens. Adv Opt Mater 2013;1:517–21.
[16] Chen X, Chen M, Mehmood MQ, et al. Longitudinal multi-foci metalens for circularly polarized light. Adv Opt Mater 2015;3:1201–6.

[17] Khorasaninejad M, Chen WT, Devlin RC, Oh J, Zhu AY, Capasso F. Metalenses at visible wavelengths: Diffraction-limited focusing and subwavelength resolution imaging. Science 2016;352:1190–4.
[18] Khorasaninejad M, Chen WT, Oh J, Capasso F. Super-dispersive off-axis meta-lenses for compact high resolution spectroscopy. Nano Lett 2016;16:3732–7.
[19] Wen D, Chen S, Yue F, et al. Metasurface device with helicity-dependent functionality. Adv Opt Mater 2016;4:321–7.
[20] Wen D, Yue F, Ardron M, Chen X. Multifunctional meta-surface lens for imaging and Fourier transform. Sci Rep 2016;6:27628.
[21] Groever B, Chen WT, Capasso F. Meta-Lens Doublet in the Visible Region. Nano Lett 2017;17:4902–7.
[22] Khorasaninejad M, Shi Z, Zhu AY, et al. Achromatic metalens over 60 nm bandwidth in the visible and metalens with reverse chromatic dispersion. Nano Lett 2017;17:1819–24.
[23] Wang S, Wu PC, Su V-C, et al. Broadband achromatic optical metasurface devices. Nat Commun 2017;8:187.
[24] Zhu AY, Chen W-T, Khorasaninejad M, et al. Ultra-compact visible chiral spectrometer with meta-lenses. APL Photonics 2017;2:036103.
[25] Arbabi E, Arbabi A, Kamali SM, Horie Y, Faraji-Dana M, Faraon A. MEMS-tunable dielectric metasurface lens. Nat Commun 2018;9:812.
[26] Chen WT, Zhu AY, Sanjeev V, et al. A broadband achromatic metalens for focusing and imaging in the visible. Nat Nanotechnol 2018;13:220–6.
[27] Groever B, Rubin NA, Mueller JPB, Devlin RC, Capasso F. High-efficiency chiral meta-lens. Sci Rep 2018;8:7240.
[28] Lee G-Y, Hong J-Y, Hwang S, et al. Metasurface eyepiece for augmented reality. Nat Commun 2018;9:4562.
[29] Pahlevaninezhad H, Khorasaninejad M, Huang Y-W, et al. Nano-optic endoscope for high-resolution optical coherence tomography in vivo. Nat Photonics 2018;12:540–7.
[30] Paniagua-Domínguez R, Yu YF, Khaidarov E, et al. A metalens with a near-unity numerical aperture. Nano Lett 2018;18: 2124–32.
[31] Wang S, Wu PC, Su V-C, et al. A broadband achromatic metalens in the visible. Nat Nanotechnol 2018;13:227–32.
[32] Zhang Z, Wen D, Zhang C, et al. Multifunctional light sword metasurface lens. ACS Photonics 2018;5:1794–9.
[33] Fu R, Li Z, Zheng G, et al. Reconfigurable step-zoom metalens without optical and mechanical compensations. Opt Express 2019;27:12221–30.
[34] Huang L, Chen X, Mühlenbernd H, et al. Three-dimensional optical holography using a plasmonic metasurface. Nat Commun 2013;4:2808.
[35] Arbabi A, Horie Y, Bagheri M, Faraon A. Dielectric metasurfaces for complete control of phase and polarization with subwavelength spatial resolution and high transmission. Nat Nanotechnol 2015;10:937.
[36] Huang Y-W, Chen WT, Tsai W-Y, et al. Aluminum plasmonic multicolor meta-hologram. Nano Lett 2015;15:3122–7.
[37] Wen D, Yue F, Li G, et al. Helicity multiplexed broadband metasurface holograms. Nat Commun 2015;6:8241.
[38] Li X, Chen L, Li Y, et al. Multicolor 3D meta-holography by broadband plasmonic modulation. Sci Adv 2016;2:e1601102.
[39] Wan W, Gao J, Yang X. Full-color plasmonic metasurface holograms. ACS Nano 2016;10:10671–80.
[40] Wang B, Dong F, Li Q-T, et al. Visible-frequency dielectric metasurfaces for multiwavelength achromatic and highly dispersive holograms. Nano Lett 2016;16:5235–40.
[41] Balthasar Mueller JP, Rubin NA, Devlin RC, Groever B, Capasso F. Metasurface polarization optics: independent phase control of arbitrary orthogonal states of polarization. Phys Rev Lett 2017;118:113901.
[42] Burch J, Wen D, Chen X, Di Falco A. Conformable holographic metasurfaces. Sci Rep 2017;7:4520.
[43] Yue F, Zang X, Wen D, et al. Geometric Phase Generated Optical Illusion. Sci Rep 2017;7:11440.
[44] Karimi E, Schulz SA, De Leon I, Qassim H, Upham J, Boyd RW. Generating optical orbital angular momentum at visible wavelengths using a plasmonic metasurface. Light Sci Appl 2014;3:e167.
[45] Yi X, Ling X, Zhang Z, et al. Generation of cylindrical vector vortex beams by two cascaded metasurfaces. Opt Express 2014;22:17207–15.
[46] Ma X, Pu M, Li X, Huang C, et al. A planar chiral metasurface for optical vortex generation and focusing. Sci Rep 2015;5:10365.
[47] Maguid E, Yulevich I, Veksler D, Kleiner V, Brongersma ML, Hasman E. Photonic spin-controlled multifunctional shared-aperture antenna array. Science 2016;352:1202.
[48] Mehmood MQ, Mei S, Hussain S, et al. Visible-frequency metasurface for structuring and spatially multiplexing optical vortices. Adv Mater 2016;28:2533–9.
[49] Yue F, Wen D, Xin J, Gerardot BD, Li J, Chen X. Vector vortex beam generation with a single plasmonic metasurface. ACS Photonics 2016;3:1558–63.
[50] Huang L, Song X, Reineke B, et al. Volumetric generation of optical vortices with metasurfaces. ACS Photonics 2017;4:338–46.
[51] Yue F, Wen D, Zhang C, et al. Multichannel polarization-controllable superpositions of orbital angular momentum states. Adv Mater 2017;29:1603838.
[52] Zhang C, Yue F, Wen D, et al. Multichannel metasurface for simultaneous control of holograms and twisted light beams. ACS Photonics 2017;4:1906–12.
[53] Si G, Zhao Y, Liu H, et al. Annular aperture array based color filter. Appl Phys Lett 2011;99:033105.
[54] Chen Q, Chitnis D, Walls K, Drysdale TD, Collins S, Cumming DRS. CMOS photodetectors integrated with plasmonic color filters. IEEE Photonic Tech L 2012;24:197–9.
[55] Yokogawa S, Burgos SP, Atwater HA. Plasmonic color filters for CMOS image sensor applications. Nano Lett 2012;12:4349–54.
[56] Jiang X, Leong ESP, Liu YJ, Si G. Tuning plasmon resonance in depth-variant plasmonic nanostructures. Mater Des 2016;96:64–7.
[57] Wang G, Chen X, Liu S, Wong C, Chu S. Mechanical chameleon through dynamic real-time plasmonic tuning. ACS Nano 2016;10:1788–94.
[58] Yue W, Gao S, Lee S-S, Kim E-S, Choi D-Y. Subtractive color filters based on a silicon-aluminum hybrid-nanodisk metasurface enabling enhanced color purity. Sci Rep 2016;6:29756.
[59] Park C-S, Shrestha VR, Yue W, et al. Structural color filters enabled by a dielectric metasurface incorporating hydrogenated amorphous silicon nanodisks. Sci Rep 2017;7:2556.
[60] Vashistha V, Vaidya G, Gruszecki P, Serebryannikov AE, Krawczyk M. Polarization tunable all-dielectric color filters based on cross-shaped Si nanoantennas. Sci Rep 2017;7:8092.

[61] Sun S, Yang W, Zhang C, et al. Real-time tunable colors from microfluidic reconfigurable all-dielectric metasurfaces. ACS Nano 2018;12:2151–9.
[62] Taghinejad M, Taghinejad H, Malak ST, et al. Sharp and tunable crystal/fano-type resonances enabled by out-of-plane dipolar coupling in plasmonic nanopatch arrays. Ann Phys (Berl) 2018;530:1700395.
[63] Lapine M, Shadrivov IV, Kivshar YS. Colloquium: nonlinear metamaterials. Rev Mod Phys 2014;86:1093–123.
[64] Kauranen M, Zayats AV. Nonlinear plasmonics. Nat Photonics 2012;6:737–48.
[65] Krasnok A, Tymchenko M, Alù A. Nonlinear metasurfaces: a paradigm shift in nonlinear optics. Mater Today 2018;21:8–21.
[66] Kivshar Y. All-dielectric meta-optics and non-linear nanophotonics. Natl Sci Rev 2018;5:144–58.
[67] Suchowski H, O'Brien K, Wong ZJ, Salandrino A, Yin X, Zhang X. Phase mismatch–free nonlinear propagation in optical zero-index materials. Science 2013;342:1223–6.
[68] Segal N, Keren-Zur S, Hendler N, Ellenbogen T. Controlling light with metamaterial-based nonlinear photonic crystals. Nat Photonics 2015;9:180–4.
[69] Almeida E, Shalem G, Prior Y. Subwavelength nonlinear phase control and anomalous phase matching in plasmonic metasurfaces. Nat Commun 2016;7:10367.
[70] Lee J, Tymchenko M, Argyropoulos C, et al. Giant nonlinear response from plasmonic metasurfaces coupled to intersubband transitions. Nature 2014;511:65–9.
[71] Celebrano M, Wu X, Baselli M, et al. Mode matching in multiresonant plasmonic nanoantennas for enhanced second harmonic generation. Nat Nanotechnol 2015;10:412–7.
[72] Klein MW, Enkrich C, Wegener M, Linden S. Second-harmonic generation from magnetic metamaterials. Science 2006;313:502–4.
[73] Linden S, Niesler FBP, Förstner J, Grynko Y, Meier T, Wegener M. Collective effects in second-harmonic generation from split-ring-resonator arrays. Phys Rev Lett 2012;109:015502.
[74] Konishi K, Higuchi T, Li J, Larsson J, Ishii S, Kuwata-Gonokami M. Polarization-controlled circular second-harmonic generation from metal hole arrays with threefold rotational symmetry. Phys Rev Lett 2014;112:135502.
[75] Liu S, Sinclair MB, Saravi S, et al. Resonantly enhanced second-harmonic generation using III–V semiconductor all-dielectric metasurfaces. Nano Lett 2016;16:5426–32.
[76] Kang L, Cui Y, Lan S, Rodrigues SP, Brongersma ML, Cai W. Electrifying photonic metamaterials for tunable nonlinear optics. Nat Commun 2014;5:4680.
[77] Shorokhov AS, Melik-Gaykazyan EV, Smirnova DA, et al. Multifold enhancement of third-harmonic generation in dielectric nanoparticles driven by magnetic fano resonances. Nano Lett 2016;16:4857–61.
[78] Ahmadivand A, Semmlinger M, Dong L, Gerislioglu B, Nordlander P, Halas NJ. Toroidal dipole-enhanced third harmonic generation of deep ultraviolet light using plasmonic meta-atoms. Nano Lett 2019;19:605–11.
[79] Kruk S, Poddubny A, Smirnova D, et al. Nonlinear light generation in topological nanostructures. Nat Nanotechnol 2019;14:126–30.
[80] Chen S, Li G, Zeuner F, et al. Symmetry-selective third-harmonic generation from plasmonic metacrystals. Phys Rev Lett 2014;113:033901.
[81] Liu H, Guo C, Vampa G, et al. Enhanced high-harmonic generation from an all-dielectric metasurface. Nat Phys 2018;14:1006–10.
[82] Liu S, Vabishchevich PP, Vaskin A, et al. An all-dielectric metasurface as a broadband optical frequency mixer. Nat Commun 2018;9:2507.
[83] Li G, Zhang S, Zentgraf T. Nonlinear photonic metasurfaces. Nat Rev Mater 2017;2:17010.
[84] Li G, Chen S, Pholchai N, et al. Continuous control of the nonlinearity phase for harmonic generations. Nat Mater 2015;14:607–12.
[85] Almeida E, Bitton O, Prior Y. Nonlinear metamaterials for holography. Nat Commun 2016;7:12533.
[86] Ye W, Zeuner F, Li X, et al. Spin and wavelength multiplexed nonlinear metasurface holography. Nat Commun 2016;7:11930.
[87] Li G, Wu L, Li KF, et al. Nonlinear metasurface for simultaneous control of spin and orbital angular momentum in second harmonic generation. Nano Lett 2017;17:7974–9.
[88] Schlickriede C, Waterman N, Reineke B, et al. Imaging through nonlinear metalens using second harmonic generation. Adv Mater 2018;30:1703843.
[89] Walter F, Li G, Meier C, Zhang S, Zentgraf T. Ultrathin nonlinear metasurface for optical image encoding. Nano Lett 2017;17:3171–5.
[90] Khorasaninejad M, Chen WT, Zhu AY, et al. Multispectral chiral imaging with a metalens. Nano Lett 2016;16:4595–600.
[91] Wu PC, Chen J-W, Yin C-W, et al. Visible metasurfaces for on-chip polarimetry. ACS Photonics 2018;5:2568–73.
[92] Rubin NA, D'Aversa G, Chevalier P, Shi Z, Chen WT, Capasso F. Matrix Fourier optics enables a compact full-Stokes polarization camera. Science 2019;365:eaax1839.
[93] Yang Z, Wang Z, Wang Y, et al. Generalized Hartmann-Shack array of dielectric metalens sub-arrays for polarimetric beam profiling. Nat Commun 2018;9:4607.
[94] Wen D, Yue F, Kumar S, et al. Metasurface for characterization of the polarization state of light. Opt Express 2015;23:10272–81.
[95] Khorasaninejad M, Crozier KB. Silicon nanofin grating as a miniature chirality-distinguishing beam-splitter. Nat Commun 2014;5:5386.
[96] Shaltout A, Liu J, Kildishev A, Shalaev V. Photonic spin Hall effect in gap-plasmon metasurfaces for on-chip chiroptical spectroscopy. Optica 2015;2:860–3.
[97] Basiri A, Chen X, Bai J, et al. Nature-inspired chiral metasurfaces for circular polarization detection and full-Stokes polarimetric measurements. Light Sci Appl 2019;8:78.
[98] Hermon S, Ma A, Yue F, et al. Metasurface hologram for polarization measurement. Opt Lett 2019;44:4436–8.
[99] Zhang X, Yang S, Yue W, et al. Direct polarization measurement using a multiplexed Pancharatnam-Berry metahologram. Optica 2019;6:1190–8.
[100] Pors A, Nielsen MG, Bozhevolnyi SI. Plasmonic metagratings for simultaneous determination of Stokes parameters. Optica 2015;2:716–23.
[101] Balthasar Mueller JP, Leosson K, Capasso F. Ultracompact metasurface in-line polarimeter. Optica 2016;3:42–7.
[102] Chen WT, Török P, Foreman MR, et al. Integrated plasmonic metasurfaces for spectropolarimetry. Nanotechnology 2016;27:224002.
[103] Pors A, Bozhevolnyi SI. Waveguide metacouplers for in-plane polarimetry. Phys Rev Appl 2016;5:064015.

[104] Ding F, Pors A, Chen Y, Zenin VA, Bozhevolnyi SI. Beam-size-invariant spectropolarimeters using gap-plasmon metasurfaces. ACS Photonics 2017;4:943–9.
[105] Maguid E, Yulevich I, Yannai M, Kleiner V, Brongersma M, Hasman E. Multifunctional interleaved geometric-phase dielectric metasurfaces. Light Sci Appl 2017;6:e17027.
[106] Wei S, Yang Z, Zhao M. Design of ultracompact polarimeters based on dielectric metasurfaces. Opt Lett 2017;42:1580–3.
[107] Arbabi E, Kamali SM, Arbabi A, Faraon A. Full-Stokes imaging polarimetry using dielectric metasurfaces. ACS Photonics 2018;5:3132–40.
[108] Lee K, Yun H, Mun S-E, Lee G-Y, Sung J, Lee B. Ultracompact broadband plasmonic polarimeter. Laser Photonics Rev 2018;12:1700297.
[109] Rubin NA, Zaidi A, Juhl M, et al. Polarization state generation and measurement with a single metasurface. Opt Express 2018;26:21455–78.
[110] Wang L, Li T, Guo RY, Xia W, Xu XG, Zhu SN. Active display and encoding by integrated plasmonic polarizer on light-emitting-diode. Sci Rep 2013;3:2603.
[111] Fuyong Y, Chunmei Z, Xiao-Fei Z, et al. High-resolution grayscale image hidden in a laser beam. Light Sci Appl 2018;7:17129.
[112] Zhang C, Wen D, Yue F, Intaravanne Y, Wang W, Chen X. Optical metasurface generated vector beam for anticounterfeiting. Phys Rev Appl 2018;10:034028.
[113] Zang X, Dong F, Yue F, et al. Polarization encoded color image embedded in a dielectric metasurface. Adv Mater 2018;30:1707499.
[114] Zhao R, Sain B, Wei Q, et al. Multichannel vectorial holographic display and encryption. Light Sci Appl 2018;7:95.
[115] Zhang C, Dong F, Intaravanne Y, et al. Multichannel metasurfaces for anticounterfeiting. Phys Rev Appl 2019;12:034028.
[116] Tang Y, Intaravanne Y, Deng J, Li KF, Chen X, Li G. Nonlinear vectorial metasurface for optical encryption. Phys Rev Appl 2019;12:024028.
[117] Chipman RA. Polarimetry. In: Bass M, editor. Handbook of Optics. Volume II: Devices, measurements, and properties, 2nd ed. USA: The McGraw-Hill Companies, Inc., 1995:22.1–22.37.
[118] Azzam RMA, Bashara NM. Ellipsometry and polarized light. Amsterdam, New York: USA, North-Holland Pub. Co., 1997.
[119] Kasic A, Schubert M, Einfeldt S, Hommel D, Tiwald TE. Free-carrier and phonon properties of n- and p-type hexagonal GaN films measured by infrared ellipsometry. Phys Rev B 2000;62:7365–77.
[120] Vasile G, Trouve E, Jong-Sen L, Buzuloiu V. Intensity-driven adaptive-neighborhood technique for polarimetric and interferometric SAR parameters estimation. IEEE Trans Geosci Remote Sens 2006;44:1609–21.
[121] Wang X, Lai J, Li Z. Polarization studies for backscattering of RBC suspensions based on Mueller matrix decomposition. Opt Express 2012;20:20771–82.
[122] Mistlberger A, Liebmann JM, Greenfield DS, et al. Heidelberg retina tomography and optical coherence tomography in normal, ocular-hypertensive, and glaucomatous eyes. Ophthalmology 1999;106:2027–32.
[123] Gansel JK, Thiel M, Rill MS, et al. Gold helix photonic metamaterial as broadband circular polarizer. Science 2009;325:1513–5.
[124] Ye Y, Li X, Zhuang F, Chang S-W. Homogeneous circular polarizers using a bilayered chiral metamaterial. Appl Phys Lett 2011;99:031111.
[125] Zhao Y, Belkin MA, Alù A. Twisted optical metamaterials for planarized ultrathin broadband circular polarizers. Nat Commun 2012;3:870.
[126] Decker M, Ruther M, Kriegler CE, et al. Strong optical activity from twisted-cross photonic metamaterials. Opt Lett 2009;34:2501–3.
[127] Rogacheva AV, Fedotov VA, Schwanecke AS, Zheludev NI. Giant gyrotropy due to electromagnetic-field coupling in a bilayered chiral structure. Phys Rev Lett 2006;97:177401.
[128] Ni X, Emani NK, Kildishev AV, Boltasseva A, Shalaev VM. Broadband light bending with plasmonic nanoantennas. Science 2012;335:427.
[129] Yu N, Genevet P, Kats MA, et al. Light propagation with phase discontinuities: generalized laws of reflection and refraction. Science 2011;334:333–7.
[130] Sun S, He Q, Xiao S, Xu Q, Li X, Zhou L. Gradient-index metasurfaces as a bridge linking propagating waves and surface waves. Nat Mater 2012;11:426–31.
[131] Huang L, Chen X, Bai B, et al. Helicity dependent directional surface plasmon polariton excitation using a metasurface with interfacial phase discontinuity. Light Sci Appl 2013;2:e70.
[132] Huang L, Chen X, Mühlenbernd H, et al. Dispersionless phase discontinuities for controlling light propagation. Nano Lett 2012;12:5750–5.
[133] Chen X, Zhang Y, Huang L, Zhang S. Ultrathin metasurface laser beam shaper. Adv Opt Mater 2014;2:978–82.